

Properties of the galaxy population in hydrodynamical simulations of clusters

A. Saro^{1,2}, S. Borgani^{1,2,3}, L. Tornatore^{4,2}, K. Dolag⁵, G. Murante^{6,1},
A. Biviano³, F. Calura³ & S. Charlot⁷

¹ Dipartimento di Astronomia dell'Università di Trieste, via Tiepolo 11, I-34131 Trieste, Italy (saro,borgani@oats.inaf.it)

² INFN – National Institute for Nuclear Physics, Trieste, Italy

³ INAF, Osservatorio Astronomico di Trieste, via Tiepolo 11, I-34131 Trieste, Italy (calura,biviano@oats.inaf.it)

⁴ SISSA/International School for Advanced Studies, via Beirut 4, 34100 Trieste, Italy (torna@sissa.it)

⁵ Max-Planck-Institut für Astrophysik, Karl-Schwarzschild Strasse 1, Garching bei München, Germany (kdolag,charlot@mpa-garching.mpg.de)

⁶ INAF, Osservatorio Astronomico di Torino, Strada Osservatorio 20, I-10025 Pino Torinese, Italy (giuseppe@to.astro.it)

⁷ Institut d'Astrophysique de Paris, CNRS, 98 bis Boulevard Arago, Paris 75014, France (charlot@iap.fr)

Accepted ???. Received ???; in original form ???

ABSTRACT

We present a study of the galaxy population predicted by hydrodynamical simulations of galaxy clusters. These simulations, which are based on the GADGET-2 Tree+SPH code, include gas cooling, star formation, a detailed treatment of stellar evolution and chemical enrichment, as well as SN energy feedback in the form of galactic winds. As such, they can be used to extract the spectro–photometric properties of the simulated galaxies, which are identified as clumps in the distribution of star particles. Simulations have been carried out for a representative set of 19 cluster–sized halos, having mass M_{200} in the range $5 \times 10^{13} - 1.8 \times 10^{15} h^{-1} M_{\odot}$. All simulations have been performed for two choices of the stellar initial mass function (IMF), namely using a standard Salpeter IMF with power–law index $x = 1.35$, and a top–heavy IMF with $x = 0.95$. In general, we find that several of the observational properties of the galaxy population in nearby clusters are reproduced fairly well by simulations. A Salpeter IMF is successful in accounting for the slope and the normalization of the color–magnitude relation for the bulk of the galaxy population. In contrast, the top–heavy IMF produces too red galaxies, as a consequence of their exceedingly large metallicity. Simulated clusters have a relation between mass and optical luminosity which generally agrees with observations, both in normalization and slope. Also in keeping with observational results, galaxies are generally bluer, younger and more star forming in the cluster outskirts. However, we find that our simulated clusters have a total number of galaxies which is significantly smaller than the observed one, falling short by about a factor 2–3. We have verified that this problem does not have an obvious numerical origin, such as lack of mass and force resolution. Finally, the brightest cluster galaxies are always predicted to be too massive and too blue, when compared to observations. This is due to gas overcooling, which takes place in the core regions of simulated clusters, even in the presence of the rather efficient supernova feedback used in our simulations.

Key words: Cosmology: numerical simulations – galaxies: clusters – hydrodynamics

1 INTRODUCTION

A key question in the study of the formation and evolution of galaxies concerns the relationship between their observational properties and the large–scale cosmological environment. In recent years, a flourishing of observational campaign has provided a detailed description of the evolution of the galaxy population in clusters. Indeed, galaxy clusters play a key role in the characterization of the galaxy evolution. Each cluster provides a large sample of galaxies, all placed at the same redshift. Furthermore, clusters offer the pos-

sibility of sampling a variety of environments, from their dense core regions, to the outskirts where the properties of the cluster galaxy population tends to approach that of the field.

A diversity of the galaxy population in nearby clusters, with respect to that in the field, was noticed already by Oemler (1974) and by Dressler (1980). Rich clusters were shown to contain a higher fraction of bulge–dominated (early type and S0) galaxies, and a correspondingly lower fraction of star forming galaxies, than poor systems. Butcher & Oemler (1978) noticed that moderately distant clusters ($z \sim 0.3$) have a galaxy popula-

tion which is generally bluer than nearby clusters. This result has been subsequently extended by a number of analyses and is currently interpreted as high redshift clusters having larger fractions of star-forming galaxies than local clusters (see Poggianti 2004, for a review). Bower et al. (1992) first noticed that early-type members of the Coma cluster lie on a tight relation in the color-magnitude diagram, a result that has been subsequently confirmed by a number of analyses for extended samples of nearby (e.g., Prugniel & Simien 1996; Andreon 2003; Barrientos et al. 2004; López-Cruz et al. 2004; McIntosh et al. 2005, and references therein) and distant clusters, out to $z \gtrsim 1$ (e.g., van Dokkum et al. 2000; Blakeslee et al. 2003; Andreon et al. 2004; Strazzullo et al. 2006, and references therein).

As for the luminosity function (LF hereafter) of cluster galaxies, much work has been done in recent years, with different groups reaching different conclusions as for its universality, shape and faint-end slope (e.g., Driver 2004, for a review). For instance, Popesso et al. (2006a) have recently analyzed the LF for sample of clusters identified in the X-ray band within the ROSAT All Sky Survey (RASS, Voges 1992) and covered by the Sloan Digital Sky Survey (SDSS Stoughton et al. 2002). They found no significant cluster to cluster variations of the LF, once calculated within the same physical radius (r_{200} or r_{500}), with a shape fitted by a double Schechter function to account for the upturn at faint magnitudes. However, these results are at variance with respect to those from other analyses (e.g., Adami et al. 2000).

Within the widely accepted standard Λ CDM cosmological scenario, galaxies arise from the hierarchical assembly of dark matter (DM) halos. The gravitational dynamics of these halos is relatively simple to describe to high precision with modern large super-computer simulations (e.g., Springel et al. 2005). However, the observational properties of galaxies are determined by the combined action of the assembly of DM halos and by the physical processes which define the evolution of the cosmic baryons. A complex interplay between radiative gas cooling, star formation, chemical enrichment and release of energy feedback from supernovae (SN) and active galactic nuclei (AGN) is expected to determine the properties of the stellar population in galaxies. At the same time, the cluster environment is expected to play a significant role in altering the evolution of galaxies. For instance, ram pressure exerted by the hot intra-cluster medium (ICM) can lead to the removal of a substantial fraction of the interstellar medium (ISM; Gunn & Gott 1972), thereby affecting galaxy morphology, star formation and luminosity (e.g., Abadi et al. 1999; Kenney et al. 2004, and references therein).

In this context, semi-analytical models of galaxy formation have been used since several years as a flexible tool to study galaxy formation within the cosmological hierarchical framework (e.g., Kauffmann et al. 1993; Somerville & Primack 1999; Cole et al. 2000; Menci et al. 2002, and references therein). A powerful implementation of this method is that based on the so-called hybrid approach, which combines N-body simulations, to accurately trace the merging history of DM halos, and semi-analytic models to describe the physics of the baryons (e.g., Kauffmann et al. 1999). Springel et al. (2001) applied this method to a DM simulation of a cluster, with high enough resolution to allow them resolving the population of dwarf galaxies. As a result, they found that several observational properties (e.g., luminosity function, mass-to-light ratio and morphological types) are rather well reproduced. Diaferio et al. (2001) applied a semi-analytical model to a DM simulation of a large cosmological box, with the aim of performing a combined study of kinematics, colors and morphologies for

both cluster and field galaxies. They concluded that a good agreement with observations holds for cluster galaxies, while colors and star formation rates of field galaxies were shown to evolve more rapidly than observed. Casagrande & Diaferio (2006) applied the same semi-analytical model to a constrained simulation of the local universe and concluded that significant differences exist between the observed and the predicted properties of the large-scale distribution of galaxy groups. De Lucia et al. (2004) incorporated in their model also a scheme of metal production to follow the enrichment of ICM and galaxies (see also Cora 2006). Among their results, they found that the color-magnitude relation (CMR) is mainly driven by metallicity effects, the redder galaxies on the sequence being on average the more metal rich. Lanzoni et al. (2005) applied their semi-analytical model to a set of DM cluster simulations. They also included a prescription to account for the effect of ram-pressure stripping of the ISM as the galaxies move in the hot cluster atmosphere, and found it to have only a very little effect on the galaxy population.

A complementary approach to the semi-analytical models is represented by using full hydrodynamical simulations, which include the processes of gas cooling and star formation. The clear advantage of this approach, with respect to semi-analytical models, is that galaxy formation can be now described by following in detail the evolution of the cosmic baryons while they follow the formation of the cosmic web. However, the limitation of this approach lies in its high computational cost, which prevents it to cover wide dynamic ranges and to sample in detail the parameter space describing the processes of star formation and feedback. For these reasons, describing the process of galaxy formation with a self-consistent hydrodynamic approach within the typical cosmological environment of ~ 10 Mpc, relevant for galaxy clusters, represents a challenging task for simulations of the present generation.

In a pioneering paper, Metzler & Evrard (1994) studied the effect of including galaxies for the energy feedback and chemical enrichment of the ICM. Since these simulations did not have enough resolution to identify galaxies, they have been placed by hand, identifying them with the peaks of the initial density field. Frenk et al. (1996) used for the first time a radiative simulation of a cluster and identified galaxies as concentrations of cooled gas. The aim of their study was to compare the dynamics of member galaxies to that of DM particles. They concluded that galaxies suffer for a substantial dynamical bias, a result which has not been confirmed by more recent hydrodynamical simulations (e.g., Faltenbacher et al. 2005; Biviano et al. 2006). Thanks to the ever improving super-computing capabilities and efficiency of simulation codes, a number of groups have recently completed hydrodynamical simulations of galaxy clusters, which have good enough resolution to trace the galaxy population with better reliability. Nagai & Kravtsov (2005) used simulations of eight groups and clusters, performed with an adaptive mesh refinement code, including star formation, feedback from supernovae and chemical enrichment, to describe the spatial distribution of galaxies inside clusters. They found that galaxies are more centrally concentrated than DM sub-halos, with their number density profile described by a NFW shape (Navarro et al. 1996), although with a smaller concentration parameter than for the DM distribution. Romeo et al. (2005) used SPH simulations of two clusters, including a similar physics, used spectrophotometric code to derive galaxy luminosities in different bands. They analyzed the resulting color-magnitude relations (CMR, hereafter) and luminosity functions, claiming for an overall general agreement with observations.

In this paper, we will present a detailed analysis of the galaxy

population for a set of 19 simulated clusters, which span the mass range from $\simeq 5 \times 10^{13} h^{-1} M_{\odot}$ to $\simeq 2 \times 10^{15} h^{-1} M_{\odot}$. The simulations have been performed with the Tree-SPH code GADGET-2 (Springel 2005). They include the effect of radiative cooling, an effective model for star formation from a multiphase ISM (Springel & Hernquist 2003a), a phenomenological recipe for galactic winds, a detailed stellar evolution model, thereby accounting also for life-times and metal production from different stellar populations (Tornatore et al. 2004; Tornatore et al. in preparation). These simulations have been carried out also by varying both the shape of the initial mass function (IMF, hereafter) and the feedback strength. The inclusion of a detailed model of chemical enrichment allows us to compute luminosities and colors for galaxies of different metallicities, by using the GALAXEV spectrophotometric code (Bruzual & Charlot 2003). In our analysis we will concentrate on the properties of galaxy clusters at $z = 0$. As we shall discuss through the paper, several observational trends are reproduced quite well by our simulations, although a number of significant discrepancies are found. For this reason, the aim of our analysis will be more that of understanding the directions to improve simulations, rather than seeking for a best fitting between model predictions and observations.

The plan of the paper is as follows. In Section 2 we provide the general characteristics of the simulated clusters and describe the relevant features of the GADGET-2 version used for this analysis. In Section 3 we will describe the method of galaxy identification and how luminosities in different bands are computed. Section 4 contains the description of the properties of the simulated galaxy population and their comparison with observational data. In particular, we will discuss the radial distribution of galaxies, the CMR, the mass-luminosity ratio, the luminosity function, the star formation rate and the color and age gradients. Our main results will be summarized and discussed in Section 5. We will discuss in an Appendix the effects of numerical resolution on the stability of the results of our analysis.

2 THE SIMULATIONS

2.1 The simulated clusters

Our set of clusters are identified within nine Lagrangian regions, centered around as many main clusters. They were extracted from a DM-only simulation with a box size of $479 h^{-1} \text{Mpc}$ of a flat Λ CDM model with $\Omega_m = 0.3$ for the matter density parameter, $h = 0.7$ for the Hubble constant in units of $100 \text{ km s}^{-1} \text{Mpc}^{-1}$, $\sigma_8 = 0.9$ for the r.m.s. fluctuation within a top-hat sphere of $8 h^{-1} \text{Mpc}$ radius and $\Omega_b = 0.04$ for the baryon density parameter (Yoshida et al. 2001).

Thanks to the fairly large size chosen for these Lagrangian regions, several of them contain other interesting clusters, besides the main one. In this way, we end up with 19 clusters with mass M_{200} in the range $5 \times 10^{13} - 1.8 \times 10^{15} h^{-1} M_{\odot}$, out of which 4 clusters have $M_{200} > 10^{15} h^{-1} M_{\odot}$ (see Table 1). Mass resolution is increased inside the interesting regions by using the Zoomed Initial Condition (ZIC) technique by Tormen et al. (1997). Unperturbed particles positions were placed on a ‘glass’ (White 1996), and initial displacements were then assigned according to the Zel-dovich approximation (e.g. Shandarin & Zel-dovich 1989). Besides

Table 1. Characteristics of the clusters identified within the simulated regions at $z = 0$. Col. 1: name of the simulated region; Col. 2: name of the clusters within each region; Col. 3: value of the total mass, M_{200} , contained within the radius r_{200} encompassing an average density 200 times larger than the critical cosmic density ρ_c (units of $10^{14} h^{-1} M_{\odot}$); Col. 4: total number of galaxies, N_{200} , within r_{200} , having a minimum number of 32 star particles.

Region name	Cluster name	M_{200}	N_{200}
g1	g1.a	12.9	418
	g1.b	3.55	149
	g1.c	1.39	51
	g1.d	0.96	33
	g1.e	0.64	35
g8	g8.a	18.4	589
	g8.b	1.02	42
	g8.c	0.67	18
	g8.d	0.59	26
	g8.e	0.54	21
g51	g51.a	10.9	371
g72	g72.a	10.7	440
	g72.b	1.55	60
g676	g676.a	0.89	23
g914	g914.a	0.86	16
g1542	g1542.a	0.89	34
g3344	g3344.a	0.97	29
g6212	g6212.a	0.92	22

the low-frequency modes, which were taken from the initial conditions of the parent simulation, the contribution of the newly sampled high-frequency modes was also added. The mass resolution was progressively degraded in more distant regions, so as to save computational resources while still correctly describing the large-scale tidal field of the cosmological environment.

Once initial conditions are created, we split particles in the high-resolution region into a DM and a gas component, whose mass ratio is set to reproduce the assumed cosmic baryon fraction. Instead of placing them on top of each other, in order to avoid spurious numerical effects, we displace gas and DM particles such that the centre of mass of each parent particle is preserved and the final gas and dark matter particle distributions are interleaved by one mean particle spacing. In the high-resolution region, the masses of the DM and gas particles are set to $m_{\text{DM}} = 1.13 \times 10^9 h^{-1} M_{\odot}$ and $m_{\text{gas}} = 1.7 \times 10^8 h^{-1} M_{\odot}$, respectively. The Plummer-equivalent softening length for the gravitational force is set to $\epsilon_{\text{P1}} = 5.0 h^{-1} \text{kpc}$, kept fixed in physical units from $z = 5$ to $z = 0$, while being $\epsilon_{\text{P1}} = 30.0 h^{-1} \text{kpc}$ in comoving units at higher redshift.

2.2 The code

Our simulations are based on an evolution of GADGET-2² (Springel et al. 2001; Springel 2005), which includes a detailed treatment of chemical enrichment from stellar evolution (Tornatore et al. 2004; Tornatore et al., in preparation). GADGET-2 is a parallel Tree+SPH code with fully adaptive time-stepping, which includes an integration scheme which explicitly conserves energy and entropy (Springel & Hernquist 2002), radiative cooling, the effect of a uniform and evolving UV background (Haardt & Madau 1996), star formation from a multiphase interstellar medium and a prescription for galactic winds triggered by

¹ We define M_{Δ} as the mass contained within a radius encompassing a mean density equal to $\Delta \rho_c$, with ρ_c the critical cosmic density.

² <http://www.MPA-Garching.MPG.DE/gadget/>

SN explosions (see Springel & Hernquist 2003a for a detailed description, SH03 hereafter), and a numerical scheme to suppress artificial viscosity far from the shock regions (see Dolag et al. (2005)). In the original version of the code, energy feedback and global metallicity were produced only by SNII under the instantaneous-recycling approximation (IRA).

We have suitably modified the simulation code, so as to correctly account for the life-times of different stellar populations, to follow metal production from both SNIa and II, while self-consistently introducing the dependence of the cooling function on metallicity by using the tables by Sutherland & Dopita (1993). A detailed description of the implementation of these algorithms will be presented in a forthcoming paper (Tornatore et al., in preparation), while we provide here a short descriptions of the most relevant features of the code.

In order to maintain the general approach of the multiphase model by SH03, we assume that stars with masses $> 40 M_{\odot}$ explode into SNII soon after their formation, thereby promptly releasing energy and metals. In contrast, we correctly account for the lifetime of stars having masses smaller than $40 M_{\odot}$. The simulations that we will discuss here use the lifetimes provided by Maeder & Meynet (1989), which have been shown to reproduce the abundance pattern in the Milky Way (Chiappini et al. 1997). Within the stochastic approach to star formation (SH03), each star particle is generated with a mass equal to one third of the mass of its parent gas particle.

Therefore, each star particle is considered as a single stellar population (SSP, hereafter), with its own mass, metallicity and redshift of formation. For each SSP we compute both the number of stars turning into SNII and Ia at each time-step and the number of stars ending their AGB phase. Then we calculate the amount of energy and metals produced by each star particle in a given time interval, decreasing accordingly the mass of the particle. In this way, each star particle is characterized by both its initial mass, assigned at the time of its formation, and its final mass, which is updated during the evolution. Both SNII and SNIa are assumed to release 10^{51} ergs each, while no energy output is associated to the mass loss from AGB stars. The relative number of SNII and SNIa depends on the choice of the stellar initial mass function (IMF). In the following, we will assume for the IMF the power-law shape $dN/d\log m \propto m^{-x}$. Simulations will be run by assuming the Salpeter IMF with $x = 1.35$ (Salpeter 1955, Sa-IMF hereafter) and a top-heavy IMF with $x = 0.95$ (Arimoto & Yoshii 1987, TH-IMF hereafter).

The SNIa are associated to binary systems whose components are in the $0.8\text{--}8 M_{\odot}$ mass range (Greggio & Renzini 1983), while SNII arise from stars with mass $> 8 M_{\odot}$. In the following, we will assume that 10 per cent of stars in the $0.8\text{--}8 M_{\odot}$ mass range belongs to binary systems, which then produces SNIa. We use the analytical fitting formulas for stellar yields of SNIa, SNII and PNe provided by Recchi et al. (2001), and based on the original nucleosynthesis computations of Nomoto et al. (1997), using their W7 model, Woosley & Weaver (1995) and Renzini & Voli (1981). The formulation for the SNIa rate has been calculated as in Matteucci & Recchi (2001). In the simulations that we present, besides H and He, we have followed Fe, O, C, Si, Mg, S. Once produced by a star particle, metals are spread over the same number of neighbours, 64, used for the SPH computations, also using the same kernel. We normalize the IMFs in the mass range $0.1\text{--}100 M_{\odot}$. Owing to the uncertainty in modelling yields for very massive stars, we take yields to be independent of mass above $40 M_{\odot}$. While any uncertainty in the yields of such massive stars has a neg-

Table 2. Characteristics of the simulations. Col. 1: simulation name; Col. 2: IMF slope; Col 3: wind speed, v_w (units of km s^{-1}).

Name	IMF slope	v_w
Sa	1.35	500
Sa-NW	1.35	0
TH	0.95	500
TH-SW	0.95	1000

ligible effect for the Salpeter IMF, their accurate description (e.g., Thielemann et al. 1996; Heger & Woosley 2002) is required when using a top-heavier IMF.

Our prescription to account for stellar evolution in the simulations implies a substantial change of the multiphase “effective model” by SH03, which we have suitably modified to account for (a) the contribution of the energy reservoir provided by the SN which are treated outside the IRA, and (b) the metal-dependence of the cooling function, that we introduce using the tables from Sutherland & Dopita (1993). The resulting density threshold for a gas particle to become multiphase, thereby being eligible to undergo star formation, is fixed to $n_H = 0.1 \text{ cm}^{-3}$ at zero metallicity. According to eq.(23) of SH03, this threshold is inversely proportional to the cooling function. Since the latter depends on metallicity, we take self-consistently a metallicity-dependent star-formation threshold for gas having a non-zero metallicity.

SH03 also provided a phenomenological description for galactic winds, which are triggered by SN energy release and whose strength is regulated by two parameters. The first one gives the wind mass loading according to the relation, $\dot{M}_W = \eta \dot{M}_*$, where \dot{M}_* is the star formation rate. Following SH03, we assume $\eta = 3$. The second parameter is the wind velocity, v_w . For the runs based on the Salpeter IMF, we always use $v_w = 500 \text{ km s}^{-1}$. For the above values of η and v_w , all the energy from SNII is converted in kinetic energy, as in the original SH03 paper. Springel & Hernquist (2003b) made a study of the star formation history predicted by hydrodynamical simulations which include galactic winds with a similar velocity. They concluded that the resulting star fraction at $z = 0$ and high- z star formation history are comparable to the observed ones. In order to verify the effect of galactic ejecta, the g676 and g51 regions are also simulated with the Salpeter IMF, but setting to zero the wind velocity (Sa-NW runs). As for the runs based on the top-heavy IMF, we will also use $v_w = 500 \text{ km s}^{-1}$ for all clusters, with the exception of g676 and g51 regions, for which we also use $v_w = 1000 \text{ km s}^{-1}$ (TH-SW runs). In this case, the two wind speeds correspond to an energy budget of about 0.4 and 1.4 times the energy provided by SNII. An efficiency larger than unity can be justified on the ground of the large uncertainties on the actual energy released by SNII explosions. In this perspective, we also take the value of the wind velocity as a confidence value. A wind velocity $v_w = 1000 \text{ km s}^{-1}$ is intended to represent an extreme feedback case, so that comparing the results with the two values of wind velocity allows us to check the effect of a stronger feedback on the final properties of the galaxy population. We summarize in Table 2 the IMFs and feedback used in our simulations.

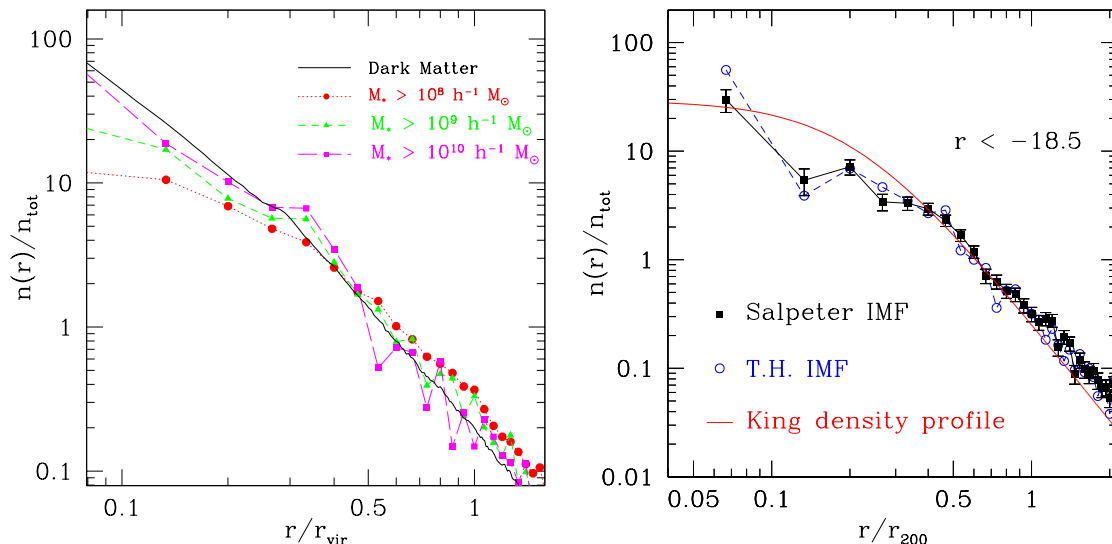


Figure 1. The number density profile of cluster galaxies. Left panel: the profiles of galaxies of different stellar mass, averaged over all clusters, for the runs with Salpeter IMF (filled symbols). Shown with the solid curve is the average DM profile. All profiles are normalized to the total number density within the virial radius. Right panel: The number density of galaxies, brighter than $r = -18.5$, contained within a given radius, normalized to the total number density found within the r_{200} . Filled squares and open circles are by combining all the simulated clusters, for the Salpeter and for the top-heavy IMF, respectively. The solid curve is the best-fit King model to the number density profiles of cluster galaxies from the analysis of RASS–SDSS data by Popesso et al. (2006b), here plotted with arbitrary normalization. Errorbars in the simulation profile correspond to Poissonian uncertainties. For reasons of clarity they have been plotted only for the Salpeter runs.

3 ASSIGNING LUMINOSITIES TO GALAXIES

As a first step, we identify galaxies from the distribution of star particles by applying the SKID algorithm³ (Stadel 2001). We provide a short description of how we applied this algorithm, while a more detailed discussion and presentation of tests is provided elsewhere (Murante et al. 2006, in preparation; see also Borgani et al. 2006). An overall density field is computed by using the distribution of all the particle species, by using a SPH spline-kernel. The star particles are then moved along the gradient of the density field in steps of $\tau/2$, where we assume $\tau \simeq 3\epsilon_{\text{PI}}$. When a particle begins to oscillate inside a sphere of radius $\tau/2$, it is stopped. Once all particles have been moved, they are grouped using a friends-of-friends (FOF) algorithm, with linking length $\tau/2$, applied to the new particle positions. The binding energy of each group identified in this way is then used to remove from the group all star particles which are recognized as unbound. All particles in a sphere of radius τ , centered on the center of mass of the group, are used to compute such a gravitational binding energy. Finally, we identify as “bona fide” galaxies only those SKID-groups containing at least 32 star particles after the removal of unbound stars.

Since each star particle is treated as a SSP, with formation redshift z_f and metallicity Z , we can assign to it luminosities in different bands by resorting to a spectrophotometric code, for the appropriate IMF used in the corresponding simulation.

To this purpose, we have used the outputs of the GALAXEV code Bruzual & Charlot (2003) to create a grid of metallicity and age values for a SSP of $1M_{\odot}$. Luminosities in different bands are then assigned to each SSP of this grid. Since two different IMFs are used for our simulations, this grid is also computed for both

the Salpeter (1955) and the top-heavy IMF. Note that GALAXEV assumes that contributions of different metal species to the total metallicity are in solar proportions, while this is not necessarily true for the star particles in our simulations. For this reason, we use the total metallicity of each star particle (i.e., the sum of the contributions from the different elements) as input for GALAXEV. We have verified that, using instead Iron or Oxygen as proxy for the global metallicity, our final results are left essentially unchanged. Consistent with the stellar evolution implemented in the simulation code, GALAXEV accounts for stellar mass loss. Therefore, we use the initial mass of each star particle in the simulations as input to GALAXEV to compute the corresponding luminosities. For each star particle we interpolate its age and metallicity with the appropriate entries of the grid. Finally, we evaluate the luminosity $L_{*,\nu}$ of each star particle, which is treated as a SSP of mass M_* and age t , in the ν band by:

$$L_{*,\nu}(t) = \frac{M_*(t)}{M_{\odot}} L_{\nu}(1M_{\odot}) \quad (1)$$

In this way, the luminosity in the ν band of each galaxy is given by the sum of the luminosities contributed by each member star particle. As a final result, for each galaxy our analysis provides stellar mass, mean stellar age, metallicity, star-formation rate (SFR), absolute magnitudes in the U, B, V, R, I, J, K , bolometric standard Johnson bands and in the g, u, r, i, z SLOAN bands.

We note that GALAXEV accounts for metallicity values in the range 0.005 – $2.6 Z_{\odot}$. While only a negligible number of stars have a metallicity below the lower limit of this interval, a sizeable number of particles, especially for the top-heavy IMF, are found with metallicities exceeding the upper limit. Whenever the particle metallicity lies outside the above range, they are set to the value of the nearest boundary.

³ See <http://www-hpcc.astro.washington.edu/tools/skid.html>

4 RESULTS

4.1 The number-density profile of cluster galaxies

A well established result from collisionless simulations of galaxy clusters is that the radial distribution of galaxy-sized subhalos is less concentrated than that of DM (e.g. Ghigna et al. 2000; Springel et al. 2001; De Lucia et al. 2004), and also less concentrated and more extended than the observed radial distribution of cluster galaxies (e.g. Diemand et al. 2004; Gao et al. 2004). While some residual numerical overmerging can still be present at the high resolution achieved in DM-only simulations, it has been suggested (Diemand et al. 2004) that overmerging may be physical in origin and related to the dissipationless dynamics. The possibility to include radiative cooling and star formation in hydrodynamical simulations allows one to verify whether the same result holds also for the galaxies identified from the star distribution. The general conclusion from these analyses is that the radial distribution of simulated galaxies is indeed more concentrated than that of DM subhalos (e.g., Nagai & Kravtsov 2005). An intermediate approach, based on coupling semi-analytical models of galaxy formation with high resolution collisionless simulations (e.g., Springel et al. 2001; Kravtsov et al. 2004; Gao et al. 2004; De Lucia et al. 2004; Lanzoni et al. 2005), confirms that the radial distribution of galaxies is more extended compared to DM. Clearly, the dynamics of halo formation in these studies is driven by the collisionless component. Therefore, suitable effective recipes should be included to prevent physical overmerging of galaxies within DM halos, so as to achieve agreement with the observed radial galaxy distribution (e.g. Springel et al. 2001; De Lucia et al. 2004).

We show in the left panel of Figure 1 the number density profiles of cluster galaxies, after averaging over all the simulated clusters, compared to the corresponding average DM density profile. As discussed by Nagai & Kravtsov (2005), selecting galaxies in hydrodynamical simulations of clusters, which include star formation, produces profiles which are generally steeper than those of DM halos. We confirm here that galaxy profiles become closer to the DM profile as more massive galaxies are selected, with objects more massive than $10^{10} h^{-1} M_{\odot}$ tracing a distribution quite close to the DM one. This is just the consequence of the improved capability of more massive galaxies to preserve their identity within merging halos. Indeed, since galaxies are more concentrated than their hosting DM halos, they are able to better survive to disruption and merging, thereby providing a better sampling of the underlying DM distribution. While this trend is generally consistent with observations, a close comparison with data requires assigning luminosities to simulated galaxies. For this reason, we also show in the right panel of Fig.1 the number density profiles of galaxies brighter that $r = -18.5$ and compare it to the best fit to the observed profiles by Popesso et al. (2006b), who trace these profiles out to $\simeq 2r_{200}$. Galaxies of this luminosity have a typical stellar mass of the order of $5 \times 10^9 M_{\odot}$ in the simulations with Salpeter IMF. In general, the observed and the simulated profiles are quite similar down to $\simeq 0.4r_{200}$. At smaller radii there is a trend for simulated galaxies to have a lower number density than in real clusters. Therefore, although tracing galaxies instead of DM halos helps in the comparison with the observed galaxy profiles, still overmerging is also the likely reason for the shallower profile as traced by simulated galaxies.

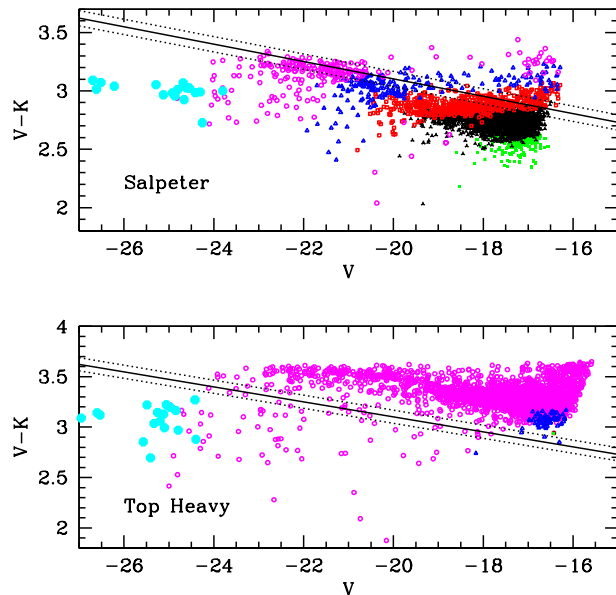


Figure 2. The $V-K$ vs. V color-magnitude relation by combining all the galaxies within the virial radii of the simulated clusters, for the Salpeter IMF (top panel) and for the top-heavy IMF with normal feedback (bottom panel). Straight lines in each panel show the observed CMR relations by Bower et al. (1992), with the corresponding intrinsic standard deviations. Big filled dots mark the BCG of each cluster. Different symbols and colors are used for galaxies having different metallicities. Magenta open circles: $Z > 1.5Z_{\odot}$; blue filled triangles: $1.5 < Z/Z_{\odot} < 1$; red open squares: $1 < Z/Z_{\odot} < 0.7$; black open triangles: $0.7 < Z/Z_{\odot} < 0.4$; green filled squares: $Z < 0.4Z_{\odot}$.

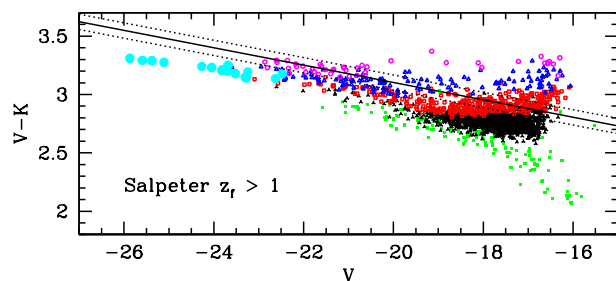


Figure 3. The same as the top panel of Figure 2, but only including in the computation of the luminosities the star particles having redshift of formation $z_f > 1$.

4.2 The color-magnitude relation

Bright massive ellipticals, which dominate the population of cluster galaxies, are observed to form a tight correlation between galaxy colors and magnitudes, the so-called red sequence or color-magnitude relation (CMR) (e.g., Bower et al. 1992; Prugniel & Simien 1996; Andreon et al. 2004; López-Cruz et al. 2004; Gladders & Yee 2005; McIntosh et al. 2005). Attempts to compare the observed CMR to that predicted by cosmological models of galaxy formation have been attempted both using semi-analytical approaches (e.g., De Lucia et al. 2004; Lanzoni et al. 2005) and full hydrodynamical simulations (Romeo et al. 2005). As a general results, model predictions reproduce the slope of the

CMR reasonably well, but with a scatter which is generally larger than observed. Romeo et al. (2005) simulated one Virgo-sized and one Coma-sized cluster. They found that a top-heavy IMF reproduces the normalization of the CMR better than a Salpeter IMF, which gives too blue colors as a consequence of the too low metallicity. This conclusion is at variance with respect to that reached by De Lucia et al. (2004) who, instead, reproduce the correct CMR normalization with a Salpeter IMF.

Thanks to the larger number of simulated clusters, we can perform the comparison between simulated and observed CMR with much improved statistics. The results of this comparison are shown in Figure 2. As a term of comparison, we use the observational determinations by Bower et al. (1992) (see also Terlevich et al. 2001) for the $V - K$ vs. V CMR, which has been determined in the magnitude range $[-18, -23]$. Quite apparently, a Salpeter IMF is successful in reproducing the correct amplitude of the CMR at the bright end, $V \lesssim -20$, while it tends to produce too blue faint galaxies. The slope of the CMR appears to be driven by metallicity, the brighter galaxies being redder mainly as a consequence of their higher metal content, thus in line with the interpretation by Kodama & Arimoto (1997). At the same time, we note that a top-heavy IMF produces too metal-rich galaxies, thereby inducing too high a normalization of the CMR.

The metal content of galaxies is clearly determined by the combined action of stellar nucleosynthesis and other processes which bring enriched gas far from star forming regions, thus preventing all metals from being locked back in newly forming stars. Processes, such as ram pressure stripping (e.g., Domainko et al. 2005) and galactic winds (e.g., Aguirre et al. 2001) have been suggested as the possible mechanisms to enrich the diffuse intergalactic medium. Clearly, the more efficient these mechanisms, the lower the expected metallicity of stars and, therefore, the bluer their colors. In order to verify whether more efficient galactic winds may decrease the metallicity of galaxies in the runs with top-heavy IMF, we have re-simulated the g676 and g51 clusters using $v_w = 1000 \text{ km s}^{-1}$ for the galactic winds (TH-SW runs). However, while the effect of the stronger feedback is that of decreasing the number of galaxies, (see also Sect. 4.4 below), it leaves their metal content, and, therefore, the high CMR normalization, almost unchanged.

Although a Salpeter IMF fares rather well as for the CMR, we note that all the BCGs (big filled circles in Fig.2) are much bluer, by about 0.5 magnitude, than expected from the red sequence. Such a blue excess of the colors of the BCGs, which takes place despite their high metallicity, finds its origin in the large star formation rate, associated to overcooling, which takes place in the central cluster regions. Typical values for the star formation rate of the BCG in our simulations are in range $600\text{--}1000 M_\odot/\text{yr}$ for the most massive clusters ($M_{200} \simeq 10^{15} h^{-1} M_\odot$) and $\sim 100 M_\odot/\text{yr}$ for the least massive ones ($M_{200} \simeq 10^{14} h^{-1} M_\odot$). Although observations indicate the presence of some ongoing star formation in some BCGs located at the center of cool core clusters, they are always at a much lower level and consistent with a star formation rate of $\sim 10\text{--}100 M_\odot/\text{yr}$ for clusters of comparable richness (e.g., Johnstone et al. 1987; Bregman et al. 2006; McNamara et al. 2006, and references therein).

The effect of recent star formation on the CMR is explicitly shown in Figure 3. We show here the case in which all star particles, formed at redshift $z < 1$ are excluded from the computation of the galaxy luminosities. This is equivalent to assume that we completely quench star formation since $z = 1$. Neglecting recent star formation has the twofold effect of reducing the scatter in the CMR

and of making BCG colors significantly redder, although they still fall slightly below the observed relation.

4.3 The mass-luminosity ratio

A number of observational analyses have established that the mass-to-light ratio in clusters generally increases with the cluster mass, $M/L \propto M^\gamma$ with $\gamma \simeq 0.2\text{--}0.4$, over a fairly large dynamic range, from poor groups to rich clusters (e.g., Adami et al. 1998; Girardi et al. 2000, 2002; Bahcall & Comerford 2002; Lin et al. 2003, 2004; Rines et al. 2004; Ramella et al. 2004; Popesso et al. 2005). A likely explanation for this trend is the reduced cooling efficiency within more massive, hotter halos (e.g., Springel & Hernquist 2003b), which reduces star formation within richer clusters. In fact, an increasing trend of M/L with cluster mass is naturally predicted by semi-analytical models of galaxy formation (e.g., Kauffmann et al. 1999).

In Figure 4 we compare the relation between mass and luminosity within r_{500} for our simulated clusters, and compare it to the i -band results by Popesso et al. (2005) and to the K -band results by Lin et al. (2004). In general, we find that the M/L from simulations is rather close to the observed one in the i band, also with a comparably small scatter. In the K band, a Salpeter IMF still agrees with observations within the statistical uncertainties, while the top-heavy IMF produces too red galaxies, thus consistent with the results of the CMR, as shown in Fig.2. We fit our mass-luminosity relation with a power-law

$$\frac{L}{10^{12} L_\odot} = \beta \left(\frac{M_{500}}{10^{14} M_\odot} \right)^\alpha, \quad (2)$$

we find $(\alpha, \beta)_i = (0.74, 0.92)$ and $(\alpha, \beta)_K = (0.76, 3.2)$ in the i and K band, respectively, for the runs with Salpeter IMF, while $(\alpha, \beta)_i = (0.70, 0.91)$ and $(\alpha, \beta)_K = (0.74, 4.7)$ for the top-heavy IMF. Therefore, our simulations agree with the observational trend for an increasing mass-to-light ratio with cluster mass, independent of the IMF and luminosity band. Using the stronger feedback for the top-heavy IMF turns into a sizeable suppression of the luminosity, especially for g51.

The reasonable level of agreement between the observed and the simulated M/L may suggest that our simulations produces a realistic population of galaxies. However, as demonstrated in Figure 5, this is not the case. In this figure, we compare the simulated and observed number of cluster galaxies, brighter than a given luminosity limit, both in i and in the K bands. Clearly, simulations underpredict such a number, by a factor $\sim 2\text{--}3$. This result is at variance with respect to that from semi-analytical models of galaxy formation, which instead predict the correct number of cluster members (e.g., De Lucia et al. 2004; Lanzoni et al. 2005). However, semi-analytical models are generally successful in producing the correct LF. They employ a suitable technique to track galaxies, based on the assumption that, once a "satellite" galaxy is formed inside a DM halo, it preserves its identity and survive to a possible disruption of the hosting halo (Springel et al. 2001). Accordingly, the position of a galaxy is later assigned to the position of the DM particle which was most bound within the DM halo before it was disrupted, thereby preventing an excessive merging rate between galaxies.

On the one hand, it is tempting to explain the lack of galaxies in our simulations as the result of an excessive merging. On the other hand, the inclusion of radiative cooling and star formation should produce galaxies in our simulations which, in fact, survive to the merging of DM halos, and behave as the "satellite" galaxies introduced in the semi-analytical models. Clearly, a reason of

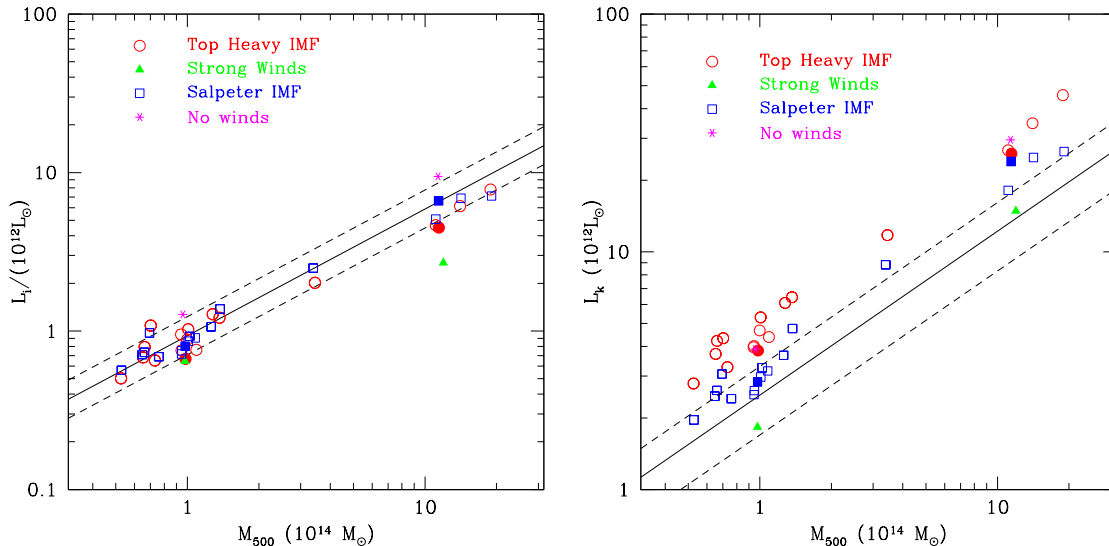


Figure 4. The comparison between simulated and observed relation between mass and luminosity in the i band (left panel) and in the K band (right panel). In each panel, squares are for the Salpeter IMF, circles for the top-heavy IMF with normal feedback, triangles for the top-heavy IMF with strong feedback and asterisks for the Salpeter IMF with no feedback. Filled squares and circles are for the g676 and g51 runs, so as to make clear the effect of changing the feedback strength. Popesso et al. (2005) for the i band and from Lin et al. (2004) for the K band, with the dashed lines marking the corresponding observational scatter.

concern in our simulations is related to the force and mass resolutions adopted (see Section 2), which may produce fragile galaxies and/or induce spurious numerical overmerging. In the Appendix we present a resolution study which is aimed at verifying whether and by how much the cluster galaxy population changes when increasing the resolution. After varying the mass resolution by a factor 45, and the corresponding softening parameters by a factor $\simeq 3.6$, we find no appreciable variations of the stellar mass function of cluster galaxies. We also verified that the lack of galaxies is not related to numerical heating induced by a non optimal choice of gravitational softening (e.g., Thomas & Couchman 1992). After running a series of simulations, using different choices for ϵ_{PI} , we find that our softening choice is very close to that maximizing the low end of the galaxy stellar mass function.

As for the effect of feedback, a wind velocity of 500 km s^{-1} is large enough to devoid the gas content of galaxies with mass $M \lesssim 10^{11} M_{\odot}$ and, therefore, to suppress the number of galaxies above the luminosity limits considered in Fig. 5. Wind velocities this high are generally expected for starburst galaxies (e.g., Heckman 2003), while they may be too high for the general galaxy population. In order to test this effect, we have performed simulations of g676 and g51 with Salpeter IMF in the extreme case in which winds are excluded. In these cases, the numbers of galaxies reported in Fig.5 increase by more than a factor of two, thus bringing simulation results into much better agreement with observational data. However, the price to pay for this is the increased total luminosities, as a result of the larger number of stars formed, which introduces a tension between simulations and observations, as shown in Fig.4. The need to reconcile at the same time the number of galaxies and the total luminosity points toward a scenario in which feedback is relatively less effective in small galaxies, while being more effective in suppressing star formation in massive rare objects. Since massive galaxies are observed to be almost passively evolving, this implies that the required feedback mechanism should not be directly linked to star formation. In this respect, AGN have

been suggested to be the natural source for this kind of feedback (e.g., Croton et al. 2006; Bower et al. 2006).

4.4 The luminosity function

The luminosity function (LF hereafter) of cluster galaxies has been the subject of numerous studies through the years (e.g., Dressler 1978; Colless 1989; Biviano et al. 1995; Goto et al. 2002; De Propris et al. 2003; Popesso et al. 2006a, , and references therein). Despite this, a general consensus on a number of issues has still to be reached. Among them, we mention the LF universality among clusters and between clusters and field, and the slope of the faint end. For instance, Popesso et al. (2006a) have recently analysed SDSS data for a set of cluster selected in the X-ray band in the RASS. As a result, they found that the LF is universal, once calculated within the same physical radius, r_{200} or r_{500} . Furthermore, the LF can not be fitted by a single Schechter (1976) function, since it displays a marked upturn at faint magnitudes. This result is at variance with other analyses. For instance, Adami et al. (2000) performed a deep spectroscopic survey of the Coma cluster and found no evidence for an upturn of the LF at faint magnitudes.

In the following, we will discuss a comparison between the LF in our simulated clusters and the observational results by Popesso et al. (2006a). To this purpose, we have computed the simulated LF, within r_{200} , in the r and z bands, which are two of the four SDSS bands where the analysis by Popesso et al. (2006a) has been performed. Consistently with their approach, we have used the procedure introduced by Colless (1989) to compute a composite luminosity function from the contribution of clusters having different richness. Accordingly, the number of galaxies N_j within the j -th luminosity bin is defined as

$$N_j = \frac{N_0}{m_j} \sum_i \frac{N_{ij}}{N_{0,i}}. \quad (3)$$

Here m_j is the number of clusters having galaxies in the j -th luminosity bin, N_{ij} is the number of galaxies in that luminosity bin

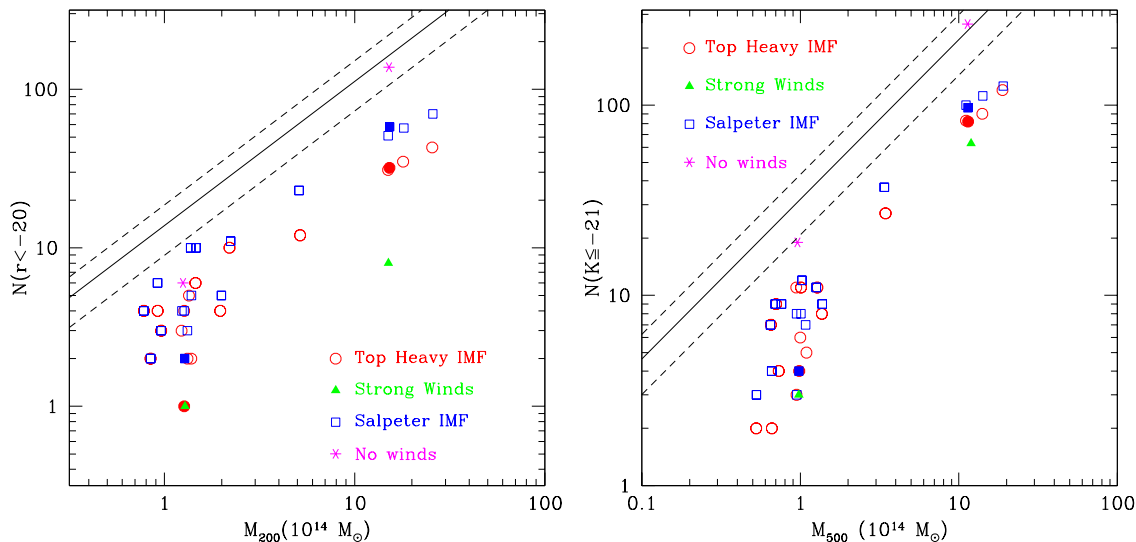


Figure 5. The number of galaxies within clusters above a given luminosity limit. Left panel: results in the r band, compared to the observational best-fitting result from SDSS data by Popesso et al. (2006b) (the dashed lines mark the intrinsic scatter of the observational relation). Right panel: results in the K band, compared to the observational best-fitting result from 2MASS data by Lin et al. (2004). Symbols for the simulations have the same meaning as in Figure 4.

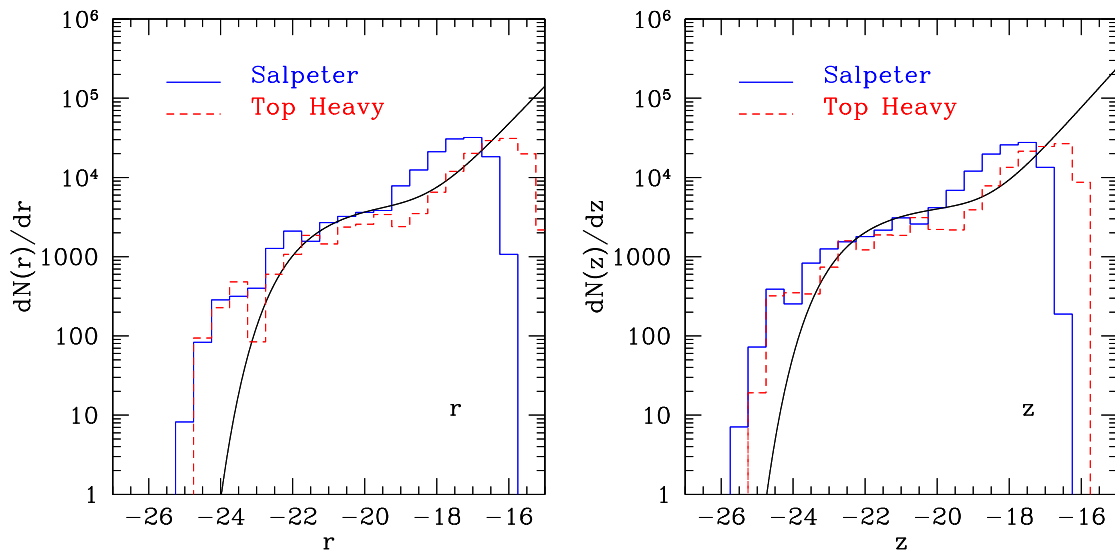


Figure 6. The Comparison between the simulated (histograms) and the observed (curves) luminosity functions of cluster galaxies in the Sloan- r (left panel) and z (right panel) bands. The smooth curves are the best fit to the SDSS data analysed by Popesso et al. (2006a). In each panel, the solid and the dashed histograms are for the Salpeter and for the top-heavy IMF, respectively. Consistent with the observational analysis, the brightest cluster galaxies (BCGs) are not included in the computation of the luminosity function.

contributed by the i -th cluster, $N_{0,i}$ is the LF normalization for the i -th cluster and $N_0 = \sum_i N_{0,i}$. Following Popesso et al. (2006a), we compute $N_{0,i}$ as the number of galaxies in the i -th cluster which are brighter than $r, z = -19$. With this definition, each cluster is weighted inversely to its richness, in such a way to avoid the richest clusters to dominate the shape of the LF. Also, consistent with Popesso et al. (2006a), we do not include the BCGs in the estimate of the LF. Owing to the too small number of galaxies found in our simulated clusters, we already know in advance that the normalization of the simulated LF must be lower than the simulated one. Therefore, we decide to normalize the simulated LF by hand, so that the LF for the Salpeter IMF matches the observed one at

$r = -20$ and $z = -20$. The resulting rescaling factor is then used also to re-normalize the LF for the runs with the top-heavy IMF. In this way, we preserve the difference in normalization between the two series of runs, which is induced by the different choices for the IMF.

The results of this comparison are shown in Figure 6. The bright end of the simulated LF is clearly shallower than that of the observed one. This is consistent with the picture that overcooling takes place within the more massive halos, which hosts the brighter galaxies. The simulated LF shows a steepening at the faint end, which resembles that found by Popesso et al. (2006a). Looking at the combined differential stellar mass function of all the cluster

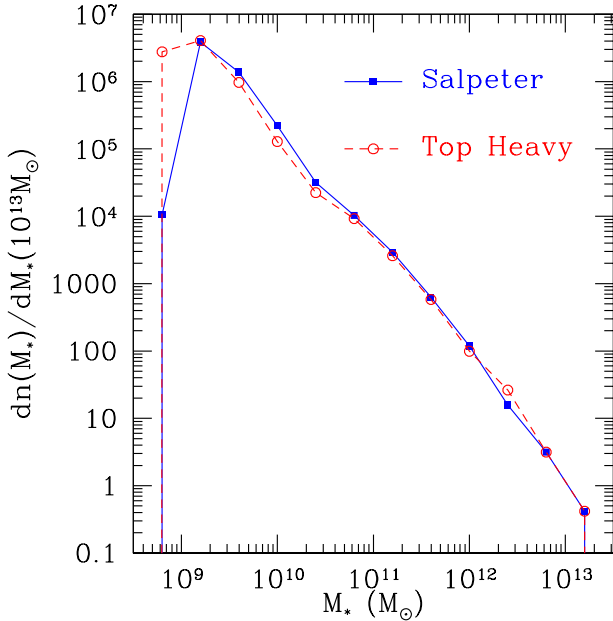


Figure 7. The combined stellar mass function for the galaxies identified within r_{200} of all clusters. The solid and the dashed histograms correspond to the Salpeter and to the top-heavy IMF, respectively.

galaxies (see Figure 7), we note an indication for a steepening of its slope at the low-mass end, $M_* \lesssim 3 \times 10^{10} M_\odot$. It is this steepening which causes the corresponding steepening of the luminosity functions. Quite interestingly, the faint end of the CMR (see Fig. 2) shows a population of small red galaxies, which are in fact associated to the excess of faint galaxies shown by the luminosity function. It is tempting to make a correspondence between these galaxies and the faint red galaxies which are claimed by Popesso et al. (2006a) to contribute to the steepening of their luminosity function. However, we consider it as premature to draw strong conclusions about the slope of the luminosity function in simulations until the latter will be demonstrated to roughly produce the correct total number of galaxies.

A comparison between the LFs produced by the Salpeter and the top-heavy IMF shows that the latter is shifted towards fainter magnitude, especially in the faint end. This effect is also visible in the corresponding stellar mass functions of the cluster galaxies (see Fig. 7). While both IMFs produces indistinguishable mass functions at the high end, galaxy masses for the top-heavy IMF tend to have lower values. This difference is induced by the larger metal content associated to the top-heavy IMF, which makes cooling more efficient within halos near the resolution limit. Finally, we show in Figure 8 the effect of increasing the feedback efficiency on the LF. In this case, we use the same normalization for the two IMFs, in order to directly see the effect of changing the feedback strength. Quite interestingly, the effect is that of suppressing the bright end of the LF, while leaving the faint end almost unaffected.

4.5 Radial dependence of the galaxy population

A number of observations have established that the galaxy population in clusters is characterized by the presence of color gradients, with bluer galaxies preferentially avoiding to reside in the innermost cluster regions (Butcher & Oemler 1984). For instance, Pimbblet et al. (2006) found a decreasing trend of the $B - R$

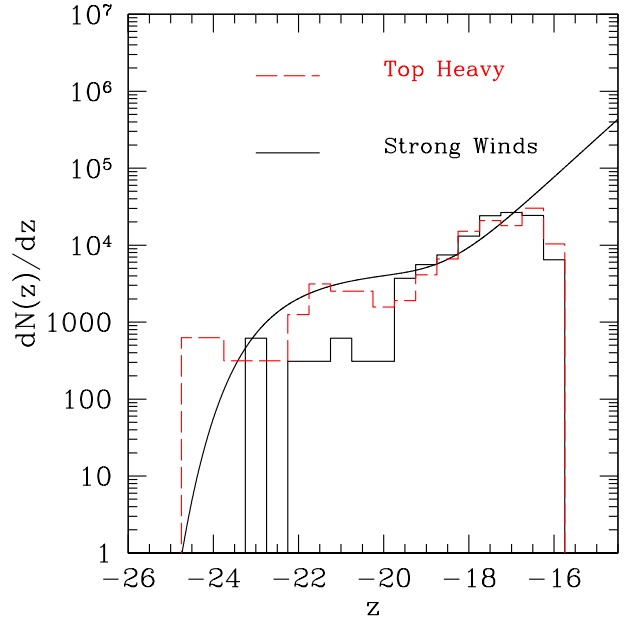


Figure 8. The effect of a stronger feedback on the z -band luminosity function. The histograms show the combined luminosity function for the g51 and g676 clusters in the case of standard feedback ($v_w = 500 \text{ km s}^{-1}$, dashed line) and of strong feedback ($v_w = 1000 \text{ km s}^{-1}$, solid line). The smooth curve is the best-fit to the SDSS data by Popesso et al. (2006a).

color with cluster-centric distance for the galaxies lying on the CMR of nearby optically selected clusters. Similar results have also been found by Abraham et al. (1996), Carlberg et al. (1997) and Wake et al. (2005) for moderately distant X-ray selected clusters. Quite consistently, outer cluster regions are populated by a larger fraction of blue galaxies (e.g., De Propris et al. 2004), thus confirming that more external galaxies are generally characterized by a relatively younger stellar population. This effect may result both as a consequence of the cluster environment, which excises star formation in infalling galaxies, and/or due to an earlier formation epoch of galaxies residing in the cluster center (e.g., Ellingson et al. 2001). In general, the presence of a gradient in the galaxy colors is naturally predicted by semi-analytical models of galaxy formation (e.g., Diaferio et al. 2001).

In Figure 9 we show the radial variation of the $B - V$ color for all galaxies found in our set of simulated clusters. Consistent with observational results, the mean galaxy colors become bluer as we move towards the outer cluster regions. Quite remarkably, this effect extends well beyond the virial radius, thus implying that galaxies feel the cluster environment already at fairly large distances. While the trend exists for both a Salpeter and a top-heavy IMF, the latter generally predicts much redder colors, consistent with the CMR results shown in Fig. 2. Our results for the Salpeter IMF are consistent with those reported by Diaferio et al. (2001) for the low-redshift bin ($0.18 < z < 0.3$) of the CNOC1 cluster sample.

We note a sudden inversion of the color gradients in the innermost regions, where galaxies are characterized by much bluer colors. These galaxies generally correspond to the cluster BCGs, which, as already discussed are much bluer than expected from the CMR red sequence (see Fig. 2). In fact, the galaxies identified in this region correspond to the BCG, which, as we have already discussed, are characterized by a strong excess of star formation. The effect is more pronounced for the top-heavy IMF, which produces

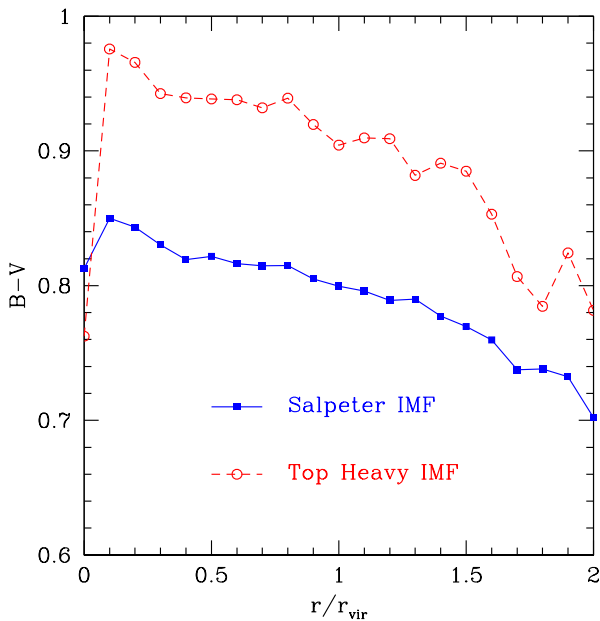


Figure 9. The radial dependence of galaxy colors, averaged over all simulated clusters. In each panel, solid lines with filled squares are for the Salpeter IMF, while dashed line with open circles are for the top-heavy IMF. The reported results are the average over all the simulated clusters.

more metals and, therefore, makes overcooling even stronger. This highlights once again the presence of too high a cooling rate at the center of the simulated clusters, which is not prevented by the model of SN feedback adopted in our simulations.

The presence of color gradients corresponds to the presence of age gradients. We show in Figure 10 the radial dependence of the fraction of galaxies younger than 8.5 Gyrs. Quite apparently, there is a continuous trend for galaxies to be younger in the outer cluster regions. The trend extends out to $2r_{\text{vir}}$, with no evidence for convergence for a stable mean age in the field. This result further confirms that the presence of a cluster induces environmental effects in the galaxy population already at quite large distances. Much like for the colors, we note an inversion of the trend in the innermost regions, which is due to the excess star formation taking place in the central BCGs. The fact that the inversion is more pronounced for the top-heavy IMF is in line with its higher enrichment, which makes gas cooling more efficient.

A consistent result also holds for the radial dependence of the star formation rate (SFR). In Figure 11 we show the specific SFR (i.e., the SFR per unit stellar mass) as a function of the cluster-centric distance. Once we exclude the contribution of the BCG in the central bin, we observe a steady increase of the SFR toward external cluster regions. In general, these results are in line with observational evidences for a younger, more star forming galaxy population in the cluster outskirts. For instance, Biviano et al. (1997) analysed the galaxy population in the ESO Nearby Abell Cluster Survey (ENACS) and found that emission-line galaxies tends to underpopulate the central regions of clusters. Balogh et al. (1997) analysed data from the CNOC1 survey of medium-distant galaxy clusters ($z \simeq 0.2-0.6$) and found evidences for a continuous increase of the SFR out to $2r_{200}$. In a similar way, Moran et al. (2005) analysed a large sample of spectroscopic data, covering a ~ 10 Mpc regions around a Cl0024 at $z \simeq 0.4$. Again, they found that galaxies appear to be younger at large radii. However, differently from our results,

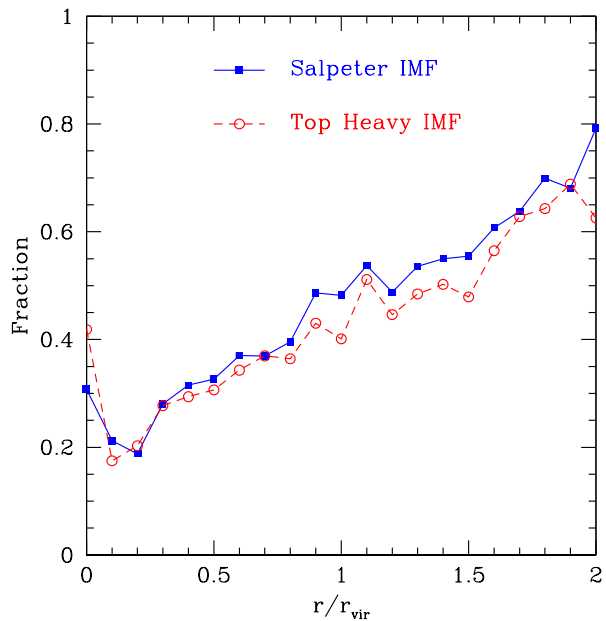


Figure 10. The fraction of galaxies younger than 8.5 Gyrs, as a function of cluster-centric distance, in units of r_{vir} . Symbols and line types have the same meaning as in Figure 9.

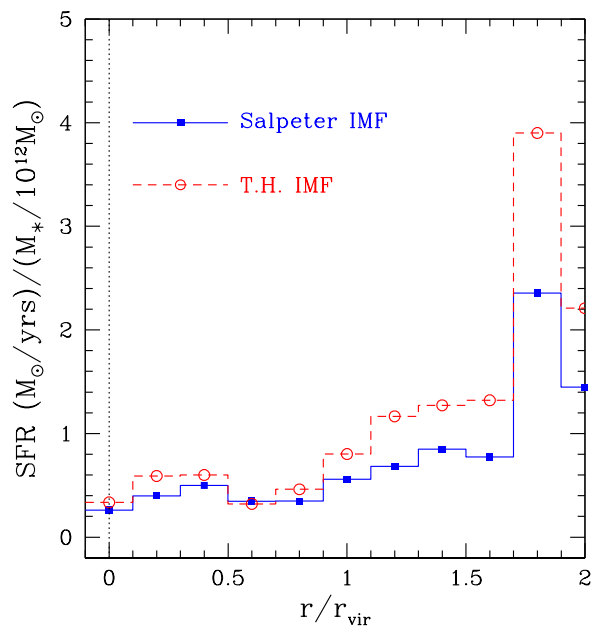


Figure 11. The specific mean star formation rate, averaged over all the simulated clusters, as a function of the cluster-centric distance. Symbols and line types have the same meaning as in Figure 9. In the central bin we have excluded the contribution from the BCGs.

they detect evidences for an increase of star formation around r_{vir} , possibly triggered by the interaction with the dense environment of the ICM.

5 CONCLUSIONS

In this paper we have presented an analysis of the galaxy population in cosmological hydrodynamical simulations of galaxy clusters at $z = 0$. The inclusion of a detailed treatment of stellar evolution and chemical enrichment (Tornatore et al. 2004; Tornatore et al., in preparation) in the GADGET-2 code (Springel 2005) has allowed us to derive the properties of galaxies in the optical/near-IR bands. In our simulations each star particle is treated as a single stellar population (SSP) characterized by a formation time and a metallicity. Based on this, we apply the GALAXEV spectro-photometric code (Bruzual & Charlot 2003) to compute luminosities in different bands. Simulations have been carried out for a representative set of galaxy clusters, containing 19 objects with mass M_{200} ranging from $5 \times 10^{13} h^{-1} M_{\odot}$ to $1.8 \times 10^{15} h^{-1} M_{\odot}$. All clusters have been simulated assuming both a standard Salpeter IMF (Salpeter 1955) and a power-law top-heavier IMF with exponent $x = 0.95$ (Arimoto & Yoshii 1987). The main results of our analysis can be summarized as follows.

1. Both the color-magnitude relation (CMR) and the M/L ratio are in reasonable agreement with observational data for a Salpeter IMF. In contrast, using a top-heavy IMF provides too high a metallicity of galaxies, which turns into too red colors. This spoils the agreement with the CMR and with the M/L ratio in the K band. The CMR is confirmed to be a metallicity sequence, in the sense that more enriched galaxies systematically populate the brighter redder part of the sequence.
2. Galaxies are systematically older and redder in central cluster regions, thus in keeping with observational results. This trend extends at least out to $2r_{vir}$, thus showing that the galaxy population feels the presence of a cluster well beyond its virial region. Due to the overcooling occurring in the central cluster regions, BCGs are always much bluer and more massive than observed, and characterized by too high a recent star formation. Indeed, neglecting the contribution of stars formed at $z < 1$ produces significantly redder BCGs, thus in better agreement with observational data.
3. The number density profile of galaxies is confirmed to steepen with the galaxy stellar mass, approaching the DM profile for the galaxies with $M_* > 10^{10} h^{-1} M_{\odot}$. However, when compared to the observations (e.g., Popesso et al. 2006b), the simulation profiles are flatter than the observed ones inside $0.4r_{200}$.
4. Simulated clusters have about three times fewer galaxies above a given luminosity limit than real clusters. We have verified that this disagreement is directly related neither to lack of mass and force resolution, nor to numerical gas heating due to a non optimal choice of the softening parameter. This leaves as further possibilities more subtle numerical effects or a better suited implementation of energy feedback.
5. The luminosity function (LF) is shallower than the observed one in the bright end, thus confirming that feedback is not strong enough to suppress cooling in the most massive halos. In the faint end, the LF steepens and indicates the presence of an excess of small red galaxies. Although this result resembles that found in observational data by Popesso et al. (2006a), we warn against its overinterpretation, in the light of the deficit of the overall number of galaxies found in the simulated clusters.

The results of our analysis support the capability of hydrodynamical simulations of galaxy clusters to reproduce the general trends characterizing their galaxy population. Therefore, simulations in which the properties of the stellar population are self-consistently predicted from the gas dynamics, can provide an alter-

native and complementary approach to semi-analytical methods. However, at present, our simulations have two main limitations in accounting for the observed properties of the cluster galaxy population.

First of all, the deficit of galaxies produced in our simulations suggests that they are not able to produce galaxies which are resistant enough to survive the tidal field of the cluster environment. Indeed, the shallow galaxy number density profile in central cluster regions shows that the problem is more apparent where effects of galaxy disruption are expected to be stronger. This result on the lack of galaxies is at variance with respect to the predictions of semi-analytical models (SAM) of galaxy formation, which produce roughly the correct number of cluster galaxies (e.g., De Lucia et al. 2004; Lanzoni et al. 2005). Comparisons between the galaxy populations predicted by hydrodynamical simulations and by SAM have shown a reasonable level of agreement. However, these comparisons have been always performed by excluding the effect of energy feedback (e.g., Helly et al. 2003; Cattaneo et al. 2006) or explicit conversion of cooled gas particles into collisionless stars (e.g., Yoshida et al. 2002).

Furthermore, we always find that the brightest cluster galaxies (BCGs) are much bluer and star forming than observed. While the adopted feedback scheme, based on galactic winds, is efficient in regulating star formation for the bulk of the galaxy population, it is not able to quench low-redshift star formation in the central cluster regions, to a level consistent with observations. Clearly, the required feedback mechanism should be such to leave the bulk of the galaxy population unaffected while acting only on the very high end of the galaxy mass distribution. Feedback from central AGN represents the natural solution and provides in principle a large enough energy budget (e.g., Rafferty et al. 2006). Its detailed implementation in cosmological hydrodynamical simulations require understanding in detail the mechanisms for the thermalization of this energy in the diffuse medium (e.g., Zanni et al. 2005; Sijacki & Springel 2006).

An ambitious goal for hydrodynamical simulations of the next generation will be that of describing in detail the complex interplay between the history of star formation and the thermodynamical and chemical evolution of the diffuse cosmic baryons. For this to be reached, it is mandatory that simulations are able to produce a realistic population of galaxies, both in terms of color and of luminosity and mass distribution. Therefore, simulation codes will be required on the one hand to have numerical effects under exquisite control and, on the other hand, to include physically motivated schemes of energy and metal feedback.

ACKNOWLEDGMENTS

The simulations were carried out at the ‘‘Centro Interuniversitario del Nord-Est per il Calcolo Elettronico’’ (CINECA, Bologna), with CPU time assigned under INAF/CINECA and University-of-Trieste/CINECA grants. We are grateful to Volker Springel, who provided us with the non public version of the GADGET-2 code. We acknowledge useful discussions with Gabriella De Lucia, Antonaldo Diaferio, Marisa Girardi, Andrey Kravtsov, Bianca Poggianti and Paola Popesso. This work has been partially supported by the PD-51 INFN grant.

REFERENCES

- Abadi M. G., Moore B., Bower R. G., 1999, *MNRAS*, 308, 947
- Abraham R. G., Smecker-Hane T. A., Hutchings J. B., Carlberg R. G., Yee H. K. C., Ellingson E., Morris S., Oke J. B., Rigler M., 1996, *ApJ*, 471, 694
- Adami C., Mazure A., Biviano A., Katgert P., Rhee G., 1998, *A&A*, 331, 493
- Adami C., Ulmer M. P., Durret F., Nichol R. C., Mazure A., Holden B. P., Romer A. K., Savine C., 2000, *A&A*, 353, 930
- Aguirre A., Hernquist L., Schaye J., Weinberg D. H., Katz N., Gardner J., 2001, *ApJ*, 560, 599
- Andreon S., 2003, *A&A*, 409, 37
- Andreon S., Willis J., Quintana H., Valtchanov I., Pierre M., Pacaud F., 2004, *MNRAS*, 353, 353
- Arimoto N., Yoshii Y., 1987, *A&A*, 173, 23
- Bahcall N. A., Comerford J. M., 2002, *ApJ*, 565, L5
- Balogh M. L., Morris S. L., Yee H. K. C., Carlberg R. G., Ellingson E., 1997, *ApJ*, 488, L75+
- Barrientos L. F., Schade D., López-Cruz O., Quintana H., 2004, *ApJS*, 153, 397
- Biviano A., Durret F., Gerbal D., Le Fevre O., Lobo C., Mazure A., Slezak E., 1995, *A&A*, 297, 610
- Biviano A., Katgert P., Mazure A., Moles M., den Hartog R., Perea J., Focardi P., 1997, *A&A*, 321, 84
- Biviano A., Murante G., Borgani S., Diaferio A., Dolag K., Girardi M., 2006, *ArXiv Astrophysics e-prints*
- Blakeslee J. P., Franx M., Postman M., et al. 2003, *ApJ*, 596, L143
- Borgani S., Dolag K., Murante G., Cheng L.-M., Springel V., Diaferio A., Moscardini L., Tormen G., Tornatore L., Tozzi P., 2006, *MNRAS*, 367, 1641
- Bower R. G., Benson A. J., Malbon R., Helly J. C., Frenk C. S., Baugh C. M., Cole S., Lacey C. G., 2006, *MNRAS*, 370, 645
- Bower R. G., Lucey J. R., Ellis R. S., 1992, *MNRAS*, 254, 601
- Bregman J. N., Fabian A. C., Miller E. D., Irwin J. A., 2006, *ArXiv Astrophysics e-prints*
- Bruzual G., Charlot S., 2003, *MNRAS*, 344, 1000
- Butcher H., Oemler A., 1978, *ApJ*, 226, 559
- Butcher H., Oemler A., 1984, *ApJ*, 285, 426
- Carlberg R. G., Yee H. K. C., Ellingson E., 1997, *ApJ*, 478, 462
- Casagrande L., Diaferio A., 2006, *ArXiv Astrophysics e-prints*
- Cattaneo A., Blaizot J., Weinberg D. H., Colombi S., Dave R., Devriendt J., Guiderdoni B., Katz N., Keres D., 2006, *ArXiv Astrophysics e-prints*
- Chiappini C., Matteucci F., Gratton R., 1997, *ApJ*, 477, 765
- Cole S., Lacey C. G., Baugh C. M., Frenk C. S., 2000, *MNRAS*, 319, 168
- Colless M., 1989, *MNRAS*, 237, 799
- Cora S. A., 2006, *MNRAS*, pp 453–+
- Croton D. J., Springel V., White S. D. M., De Lucia G., Frenk C. S., Gao L., Jenkins A., Kauffmann G., Navarro J. F., Yoshida N., 2006, *MNRAS*, 365, 11
- De Lucia G., Kauffmann G., Springel V., White S. D. M., Lanzoni B., Stoehr F., Tormen G., Yoshida N., 2004, *MNRAS*, 348, 333
- De Lucia G., Kauffmann G., White S. D. M., 2004, *MNRAS*, 349, 1101
- De Propris R., Colless M., Driver S. P., et al. 2003, *MNRAS*, 342, 725
- De Propris R., Colless M., Peacock J. A., et al. 2004, *MNRAS*, 351, 125
- Diaferio A., Kauffmann G., Balogh M. L., White S. D. M., Schade D., Ellingson E., 2001, *MNRAS*, 323, 999
- Diemand J., Moore B., Stadel J., 2004, *MNRAS*, 352, 535
- Dolag K., Vazza F., Brunetti G., Tormen G., 2005, *MNRAS*, 364, 753
- Domainko W., Mair M., Kapferer W., van Kampen E., Kronberger T., Schindler S., Kimeswenger S., Ruffert M., Mangete O. E., 2005, *ArXiv Astrophysics e-prints*
- Dressler A., 1978, *ApJ*, 223, 765
- Dressler A., 1980, *ApJ*, 236, 351
- Driver S., 2004, *Publications of the Astronomical Society of Australia*, 21, 344
- Ellingson E., Lin H., Yee H. K. C., Carlberg R. G., 2001, *ApJ*, 547, 609
- Faltenbacher A., Kravtsov A. V., Nagai D., Gottlöber S., 2005, *MNRAS*, 358, 139
- Frenk C. S., Evrard A. E., White S. D. M., Summers F. J., 1996, *ApJ*, 472, 460
- Gao L., De Lucia G., White S. D. M., Jenkins A., 2004, *MNRAS*, 352, L1
- Ghigna S., Moore B., Governato F., Lake G., Quinn T., Stadel J., 2000, *ApJ*, 544, 616
- Girardi M., Borgani S., Giuricin G., Mardirossian F., Mezzetti M., 2000, *ApJ*, 530, 62
- Girardi M., Manzato P., Mezzetti M., Giuricin G., Limboz F., 2002, *ApJ*, 569, 720
- Gladders M. D., Yee H. K. C., 2005, *ApJS*, 157, 1
- Goto T., Okamura S., McKay T. A., Bahcall N. A., Annis J., Bernard M., Brinkmann J., Gómez P. L., Hansen S., Kim R. S. J., Sekiguchi M., Sheth R. K., 2002, *PASJ*, 54, 515
- Greggio L., Renzini A., 1983, *A&A*, 118, 217
- Gunn J. E., Gott J. R. I., 1972, *ApJ*, 176, 1
- Haardt F., Madau P., 1996, *ApJ*, 461, 20
- Heckman T. M., 2003, in Avila-Reese V., Firmani C., Frenk C. S., Allen C., eds, *Revista Mexicana de Astronomia y Astrofisica Conference Series Starburst-Driven Galactic Winds*. pp 47–55
- Heger A., Woosley S. E., 2002, *ApJ*, 567, 532
- Helly J. C., Cole S., Frenk C. S., Baugh C. M., Benson A., Lacey C., Pearce F. R., 2003, *MNRAS*, 338, 913
- Johnstone R. M., Fabian A. C., Nulsen P. E. J., 1987, *MNRAS*, 224, 75
- Kauffmann G., Colberg J. M., Diaferio A., White S. D. M., 1999, *MNRAS*, 303, 188
- Kauffmann G., White S. D. M., Guiderdoni B., 1993, *MNRAS*, 264, 201
- Kenney J. D. P., van Gorkom J. H., Vollmer B., 2004, *AJ*, 127, 3361
- Kodama T., Arimoto N., 1997, *A&A*, 320, 41
- Kravtsov A. V., Berlind A. A., Wechsler R. H., Klypin A. A., Gottlöber S., Allgood B., Primack J. R., 2004, *ApJ*, 609, 35
- Lanzoni B., Guiderdoni B., Mamon G. A., Devriendt J., Hatton S., 2005, *MNRAS*, 361, 369
- Lin Y.-T., Mohr J. J., Stanford S. A., 2003, *ApJ*, 591, 749
- Lin Y.-T., Mohr J. J., Stanford S. A., 2004, *ApJ*, 610, 745
- López-Cruz O., Barkhouse W. A., Yee H. K. C., 2004, *ApJ*, 614, 679
- Maeder A., Meynet G., 1989, *A&A*, 210, 155
- Matteucci F., Recchi S., 2001, *ApJ*, 558, 351
- McIntosh D. H., Zabludoff A. I., Rix H.-W., Caldwell N., 2005, *ApJ*, 619, 193
- McNamara B. R., Rafferty D. A., Birzan L., Steiner J., Wise M. W., Nulsen P. E. J., Carilli C. L., Ryan R., Sharma M., 2006, *ArXiv Astrophysics e-prints*

- Menci N., Cavaliere A., Fontana A., Giallongo E., Poli F., 2002, *ApJ*, 575, 18
- Metzler C. A., Evrard A. E., 1994, *ApJ*, 437, 564
- Moran S. M., Ellis R. S., Treu T., Smail I., Dressler A., Coil A. L., Smith G. P., 2005, *ApJ*, 634, 977
- Nagai D., Kravtsov A. V., 2005, *ApJ*, 618, 557
- Navarro J., Frenk C., White S., 1996, *ApJ*, 462, 563
- Nomoto K., Iwamoto K., Nakasato N., Thielemann F.-K., Brachwitz F., Tsujimoto T., Kubo Y., Kishimoto N., 1997, *Nuclear Physics A*, 621, 467
- Oemler A. J., 1974, *ApJ*, 194, 1
- Pimbblet K. A., Smail I., Edge A. C., O’Hely E., Couch W. J., Zabudoff A. I., 2006, *MNRAS*, 366, 645
- Poggianti B., 2004, in Dettmar R., Klein U., Salucci P., eds, *Baryons in Dark Matter Halos Evolution of galaxies in clusters*
- Popesso P., Biviano A., Böhringer H., Romaniello M., 2006a, *A&A*, 445, 29
- Popesso P., Biviano A., Böhringer H., Romaniello M., 2006b, *ArXiv Astrophysics e-prints*
- Popesso P., Biviano A., Böhringer H., Romaniello M., Voges W., 2005, *A&A*, 433, 431
- Prugniel P., Simien F., 1996, *A&A*, 309, 749
- Rafferty D. A., McNamara B. R., Nulsen P. E. J., Wise M. W., 2006, *ArXiv Astrophysics e-prints*
- Ramella M., Boschini W., Geller M. J., Mahdavi A., Rines K., 2004, *AJ*, 128, 2022
- Recchi S., Matteucci F., D’Ercole A., 2001, *MNRAS*, 322, 800
- Renzini A., Voli M., 1981, *A&A*, 94, 175
- Rines K., Geller M. J., Diaferio A., Kurtz M. J., Jarrett T. H., 2004, *AJ*, 128, 1078
- Romeo A. D., Portinari L., Sommer-Larsen J., 2005, *MNRAS*, 361, 983
- Salpeter E. E., 1955, *ApJ*, 121, 161
- Schechter P., 1976, *ApJ*, 203, 297
- Shandarin S. F., Zeldovich Y. B., 1989, *Reviews of Modern Physics*, 61, 185
- Sijacki D., Springel V., 2006, *MNRAS*, 366, 397
- Somerville R. S., Primack J. R., 1999, *MNRAS*, 310, 1087
- Springel V., 2005, *MNRAS*, 364, 1105
- Springel V., Hernquist L., 2002, *MNRAS*, 333, 649
- Springel V., Hernquist L., 2003a, *MNRAS*, 339, 289
- Springel V., Hernquist L., 2003b, *MNRAS*, 339, 312
- Springel V., White S., Tormen G., Kauffmann G., 2001, *MNRAS*, 328, 726
- Springel V., White S. D. M., Jenkins A., Frenk C. S., Yoshida N., Gao L., Navarro J., Thacker R., Croton D., Helly J., Peacock J. A., Cole S., Thomas P., Couchman H., Evrard A., Colberg J., Pearce F., 2005, *Nature*, 435, 629
- Springel V., Yoshida N., White S., 2001, *New Astronomy*, 6, 79
- Stadel J. G., 2001, Ph.D. Thesis
- Stoughton C., Lupton R. H., Bernardi M., et al. 2002, *AJ*, 123, 485
- Strazzullo V., Rosati P., Stanford S. A., Lidman C., Nonino M., Demarco R., Eisenhardt P. E., Ettori S., Mainieri V., Toft S., 2006, *ArXiv Astrophysics e-prints*
- Sutherland R. S., Dopita M. A., 1993, *ApJS*, 88, 253
- Terlevich A. I., Caldwell N., Bower R. G., 2001, *MNRAS*, 326, 1547
- Thielemann F.-K., Nomoto K., Hashimoto M.-A., 1996, *ApJ*, 460, 408
- Thomas P. A., Couchman H. M. P., 1992, *MNRAS*, 257, 11
- Tormen G., Bouchet F. R., White S. D. M., 1997, *MNRAS*, 286, 865
- Tornatore L., Borgani S., Matteucci F., Recchi S., Tozzi P., 2004, *MNRAS*, 349, L19
- van Dokkum P. G., Franx M., Fabricant D., Illingworth G. D., Kelson D. D., 2000, *ApJ*, 541, 95
- Voges W., 1992, in *Environment observation and climate modelling through international space projects. Space sciences with particular emphasis on high-energy astrophysics The rosat all-sky x-ray survey*. ESA, p. 9
- Wake D. A., Collins C. A., Nichol R. C., Jones L. R., Burke D. J., 2005, *ApJ*, 627, 186
- White S., 1996, in Schaeffer R., Silk J., Spiro M., Zinn-Justin J., eds, *Cosmology and Large-Scale Structure The formation and evolution of galaxies*. Elsevier, Dordrecht, p. 395
- Woolsey S. E., Weaver T. A., 1995, *ApJS*, 101, 181
- Yoshida N., Sheth R. K., Diaferio A., 2001, *MNRAS*, 328, 669
- Yoshida N., Stoehr F., Springel V., White S., 2002, *MNRAS*, 334, 762
- Zanni C., Murante G., Bodo G., Massaglia S., Rossi P., Ferrari A., 2005, *A&A*, 429, 399

APPENDIX. TESTING NUMERICAL EFFECTS ON THE GALAXY STELLAR MASS FUNCTION

In this Appendix we discuss the stability, against possible numerical effects, of the stellar mass function of the galaxies identified inside simulated clusters. In particular, we will focus the analysis on (a) the effect of changing the softening of the gravitational force, to control the possible presence of spurious numerical heating (e.g., Thomas & Couchman 1992); (b) the effect of mass and force resolution. As for the softening choice, it is known that using too small values may induce spurious heating of the gas particles by two-body collisions, thereby inhibiting gas cooling inside small halos. On the other hand, increasing it to too large a value also reduces the number of galaxies as a consequence of the lower number of resolved small halos (Borgani et al. 2006). As for the resolution, increasing it has the effect to better resolve the low end of the mass function and, in general, is expected to produce a more reliable galaxy population.

The tests described in this Appendix are based on three cluster sized halos, which have been resimulated by varying mass and force resolution. These clusters have virial masses in the range $(1.6\text{--}2.9) \times 10^{14} h^{-1} M_{\odot}$ and are described in detail by Borgani et al. (2006). They have been simulated for the same cosmological model of the clusters described in this paper, but with a lower normalization of the power spectrum, $\sigma_8 = 0.8$. At the lowest resolution, the mass of the gas particle is $m_{\text{gas}} \simeq 6.9 \times 10^8 h^{-1} M_{\odot}$ and the Plummer-equivalent softening for gravitational forces is set to $\epsilon = 7.5 h^{-1} \text{kpc}$ at $z = 0$. We point out that the simulations analysed in this paper and described in Section 2.1 have a mass resolution which is better than the above one by about a factor of four. Runs at increasingly higher resolution have been performed by decreasing the particle masses by a factor 3, 10 and 45, with the softening correspondingly decreased according to the $m^{1/3}$ scaling. Therefore, at the highest resolution, it is $m_{\text{gas}} \simeq 1.5 \times 10^7 h^{-1} M_{\odot}$ and $\epsilon = 2.1 h^{-1} \text{kpc}$. This mass resolution is $\simeq 11$ times higher than used for the set of simulations analysed in this paper. For the most massive of these three clusters, we have also repeated the simulation at 10 times the basic mass resolution with four different choices of the gravitational softening. In particular, we have decreased it by a factor two, with respect to

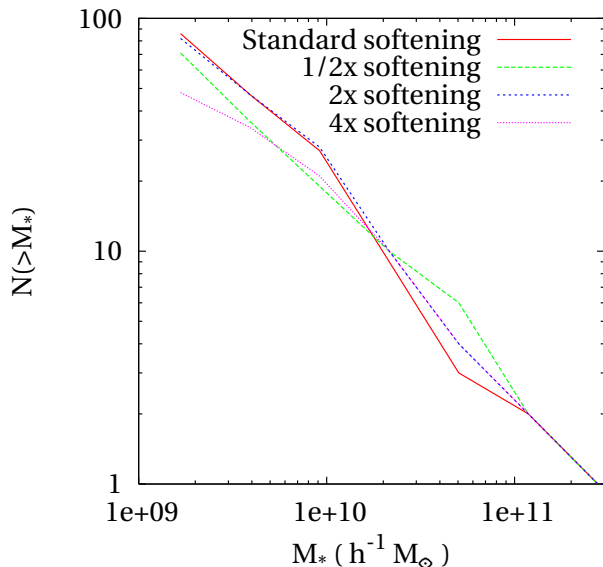


Figure 12. The cumulative stellar mass function of the galaxies identified within the virial radii of the most massive among the three simulated clusters described in the Appendix (see also Borgani et al. 2006). All the simulations have been done at fixed mass resolution, which correspond to an increase by a factor 10 with respect to the basic resolution (i.e., $m_{\text{gas}} \simeq 6.9 \times 10^7 h^{-1} M_{\odot}$; see text). The four curves correspond to the different choices for the gravitational softening. The labels indicate the factor by which the softening has been changed, with respect to the standard choice of $3.5 h^{-1} \text{kpc}$.

the standard choice, and increased it by a factor two and four. As such, this set of simulations allows us to verify the stability of the galaxy stellar mass function against changing mass resolution and the choice for the gravitational softening.

The simulations have been performed with the original prescription for star formation and feedback presented by Springel & Hernquist (2003a), with a wind speed $v_w \simeq 480 \text{ km s}^{-1}$, therefore comparable to that assumed for the standard feedback in this paper. However, those runs did not include the prescription for stellar evolution and chemical enrichment, which we used here. Since each gas particle is allowed to spawn two star particles, the latter have a mass which is half of that of the parent gas particle. As discussed by Borgani et al. (2006), this series of runs produces an amount of stars within the virial radius of the clusters, which is almost independent of the resolution, thereby preventing the runaway of cooling with increasing resolution.

We show in Figure 12 the effect of varying the softening on the cumulative stellar mass function of the galaxies identified inside the virial radius. As expected, decreasing the softening to half the standard value has the effect of suppressing the low end of the mass function, $M_* \lesssim 2 \times 10^{10} h^{-1} M_{\odot}$, as a consequence of spurious numerical heating of gas. On the other hand, increasing the softening by a factor four also induces a suppression of low-mass galaxies, as a consequence of the lack of resolution. At larger masses, using a too small softening has the effect of increasing the mass function, although the rather small number of galaxies in the high mass end prevents from detecting systematic trends. These results demonstrate that our lack of galaxies can not be explained by a non-optimal choice of the gravitational force softening.

As for the effect of resolution, we plot in Figure 13 the combined cumulative stellar mass function for all the galaxies identi-

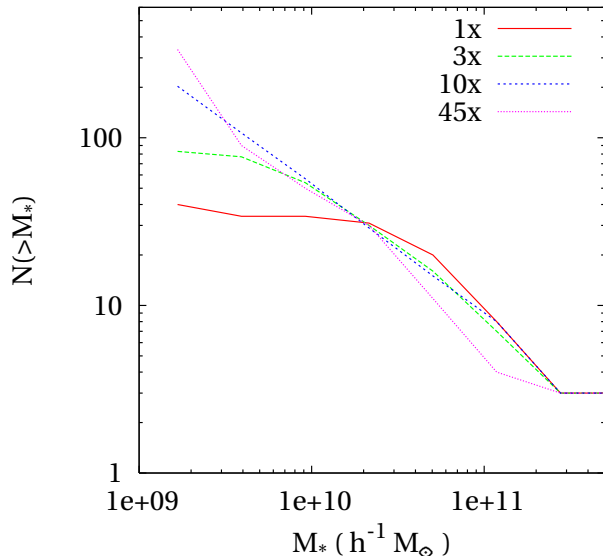


Figure 13. The combined cumulative stellar mass function of the galaxies identified within the virial radii of the three clusters. The four curves correspond to the different resolutions at which the clusters have been simulated. Continuous, long-dashed, short-dashed and dotted curves are for the simulations at progressively increasing resolution. The labels indicate the factor by which mass resolution is increased, with respect to the lowest resolution run (1x).

fied within the virial radii of the three clusters, simulated at four different resolutions. The first apparent effect of increasing resolution is that of steepening the mass function in the low mass end. In the mass range where galaxies are identified with at least 64 star particles at the different resolutions, which correspond to $M_* \simeq 2.2 \times 10^{10} h^{-1} M_{\odot}$ for the lowest resolution run, the mass functions have a weaker dependence on resolution, with a decreasing trend of the high end of the mass function. This steepening of the high end of the mass function at increasing resolution is the consequence of the reduction of overmerging, which makes small halos surviving more efficiently and, therefore, prevents their disruption and accretion inside massive halos. This result demonstrates that, at least at the highest resolution reached in this test, also resolution is not the reason for the too low number of galaxies found in the simulated clusters, when compared to observations (see discussion in Sect. 4.3).